Journal of ELECTRONIC MATERIALS, Vol. 47, No. 8, 2018
https://doi.org/10.1007/s11664-018-6178-9
© 2018 The Minerals, Metals & Materials Society

TOPICAL COLLECTION: ELECTRONIC MATERIALS FOR RENEWABLE ENERGY APPLICATIONS

Structural, Optical, and Vibrational Properties of ZnO Microrods Deposited on Silicon Substrate

BASHAR I. LAHLOUH,[1,3] SHADIA J. IKHMAYIES,[2,4] and HASSAN K. JUWHARI[1,5]

1.—School of Science, Department of Physics, University of Jordan, Amman 11942, Jordan. 2.—Faculty of Science, Physics Department, Al Isra University, Amman 11622, Jordan. 3.—e-mail: bashar_lahlouh@ju.edu.jo. 4.—e-mail: shadia_ikhmayies@yahoo.com. 5.—e-mail: h.juwhari@ju.edu.jo

Zinc oxide (ZnO) microrod films deposited by spray pyrolysis on silicon substrate at 350 ± 5°C have been studied and evaluated, and compared with thin films deposited by electron beam to confirm the identity of the studied samples. The films were characterized using different techniques. The microrod structure was studied and confirmed by scanning electron microscopy. Fourier-transform infrared (FTIR) spectroscopy and x-ray diffraction analysis confirmed successful deposition of ZnO thin films with the expected wurtzite structure. Reflectance data showed a substantial drop across the whole studied wavelength range. The photoluminescence (PL) spectra of the studied samples showed a peak at ~ 360 nm, representing a signature of ZnO. The shift in the PL peak position is due to defects and other species present in the films, as confirmed by FTIR and energy-dispersive x-ray spectroscopy results.

Key words: ZnO microrods, spray pyrolysis, thin films, solar cells

INTRODUCTION

Zinc oxide (ZnO) is a metal-oxide semiconductor with a direct, wide bandgap energy (E_g) of 3.37 eV at room temperature.[1,2] ZnO is a technologically important material for use in devices ranging from solar cells to ultraviolet (UV) light-emitting/detecting devices and pressure/gas sensor applications.[1–7] Electrodes made of ZnO, among many other materials, are also attractive for use in dye-sensitized solar cells and as anodes of lithium-ion batteries.[3,6,7] ZnO crystallizes in wurtzite structure with lattice constants c = 5.21 Å and a = 3.25 Å.[3] It exhibits strong piezoelectric properties when the c-axis is oriented perpendicular to the supporting substrate.[4] Due to its high room-temperature exciton binding energy (60 meV), ZnO shows promise for use in UV lasing and optical detection.[5] The effects of quantum confinement on the properties of this material are also studied, as controlled nanocrystalline structures of this material have been developed. However, controlling the size, shape, and morphology of such micro- and nanostructures is challenging, especially when using low-cost and relatively simple deposition methods. Thin films of zinc oxide with micro/nanostructure can be prepared using various methods, including the sol–gel method,[3,8] the hydrothermal method,[9] molecular beam epitaxy,[10] chemical vapor deposition (CVD),[11] metalorganic chemical vapor deposition (MOCVD),[12–14] magnetron sputtering,[15] and spray pyrolysis (SP).[4–23] However, in terms of low-cost, large-scale production and the ability to tune the film properties by controlling various deposition parameters, the SP method is advantageous. This paper presents preliminary results on the structure, morphology, composition, and vibrational and optical properties of ZnO microrods produced as thin films on silicon substrate using the spray pyrolysis (SP) method.

EXPERIMENTAL PROCEDURES

Microrod-structured ZnO thin films were produced on silicon substrate by spray pyrolysis (SP)

(Received November 2, 2017; accepted February 23, 2018; published online March 8, 2018)

technique at substrate temperature of 350 ± 5°C. Boron-doped *p*-type, 3 Ω cm to 30 Ω cm, (100) orientation, single-side-polished, 675 ± 25 μm-thick silicon (Si) substrate with area of 5 mm × 5 mm were cut from a 150-mm wafer (Semiconductor Wafer, Inc.). Prior to deposition, the wafers were cleaned in acetone, methanol, and deionized (DI) water, and blown dry. The starting material was zinc chloride ($ZnCl_2$) of 99% purity. By dissolving 2.5 g $ZnCl_2$ in 60 ml distilled water, 0.03 M precursor solution was prepared. Using air as carrier gas, spraying was carried out intermittently in vertical fashion on heated Si substrate. At the end of deposition, the heater was turned off and the samples were kept on the heater to cool down gradually to room temperature.

An SCT-1800 electron beam (EB) system (System Control Technologies) was also used to deposit ∼ 45-nm ZnO thin films on Si substrate as a reference control sample. ZnO powder (99.9%) was first pressed into uniform disks, which were loaded into the tungsten EB liner. The deposited films were annealed in air in a Dentsply muffle furnace at 300°C for 1 h and left to cool down overnight.

X-ray diffraction (XRD) patterns were measured using a Shimadzu diffractometer (model 7000) with Cu K_α radiation (λ = 1.54 Å) at step size of 0.02° and scan speed of 2°/min, in continuous 2θ mode in the range from 25° to 60° at current of 30 mA and voltage of 40 kV. Film morphology was examined by scanning electron microscopy (SEM, Inspect F50, FEI) equipped with an energy-dispersive x-ray spectroscopy (EDS) attachment (Bruker). To avoid any charging problems in the SEM, each film was coated with a thin platinum layer. The composition was explored by x-ray fluorescence (XRF) using a Shimadzu XRF-1800. Chemical bonding was examined by Fourier-transform infrared (FTIR) measurements, using a Thermo Nicolet Nexus 670 FT-IR spectrometer (Thermo Electron Corp.). The optical reflectance was measured at room temperature using a FilmTek 3000, which is capable of measuring both percent reflectance (*R*%) and percent transmittance (*T*%) at normal incidence in the wavelength range from 240 nm to 840 nm. The measured data were then fit using different material models, yielding the film thickness. Sample 1 had thickness of ∼ 200 nm, while sample 2 had thickness of ∼ 120 nm. The photoluminescence (PL) spectra for the two samples were recorded at room temperature using a Cary Eclipse (Varian) spectrofluorometer with a xenon lamp (wavelength of 300 nm) as excitation source. The slits of the spectral excitation and emission monochromators were both kept open at 5 nm during all PL measurements. PL data were recorded in the range from 330 nm to 570 nm. ImageJ software was used to estimate the size distribution of the microrods.[24,25]

RESULTS AND DISCUSSION

Figure 1 shows the XRD patterns of the microrod-structured ZnO films prepared at substrate temperature T = 350 ± 5°C on Si substrate. The films were polycrystalline in nature with well-defined diffraction peaks corresponding to reflections from (100), (002), (101), and (102) planes of the hexagonal wurtzite-type crystal structure of ZnO in Joint Committee on Powder Diffraction Standards (JCPDS) card no. 36-1451. The films exhibited a high-intensity (002) diffraction peak, indicating *c*-oriented ZnO films. Increase of the (002) orientation of the hexagonal wurtzite crystal structure influences both the electrical conductivity and optical properties of ZnO thin films,[26–30] and strengthens the piezoelectric properties.[4] The relative intensity ratio $I(002)/I(101)$ was 3.76 for sample 1 (t = 200 nm) and 8.82 for sample 2 (t = 120 nm), i.e., larger for the thinner sample.

Figure 2 shows the XRD diffractogram of the EB-deposited thin films, showing three easily identifiable major peaks corresponding to reflections from (001), (002), and (101) planes. This makes the EB-deposited sample a good control reference to confirm other measurements done on the SP-deposited samples.

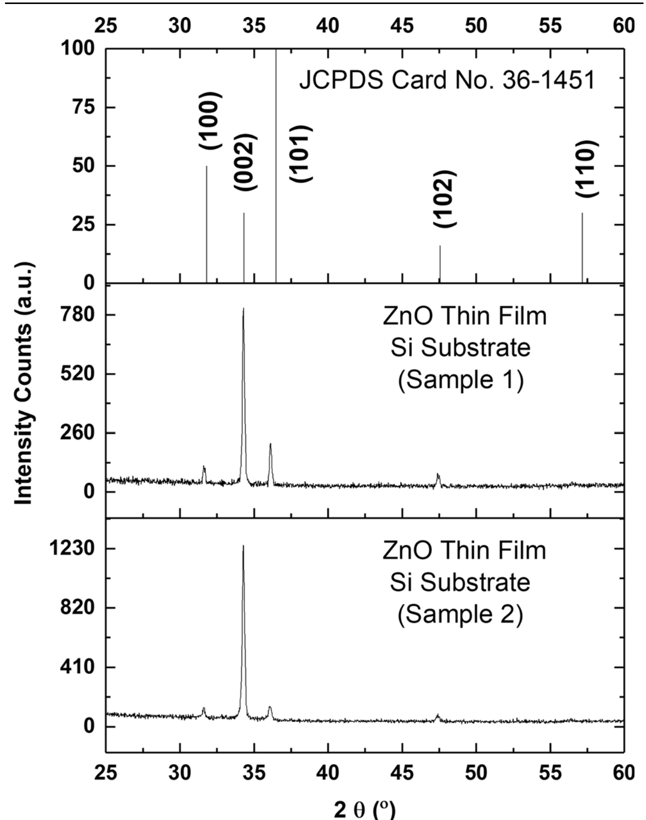

Fig. 1. XRD diffractogram of two as-deposited ZnO thin films on silicon substrate in addition to diffractogram of powder ZnO file in JCPDS card no. 00-036-1451.

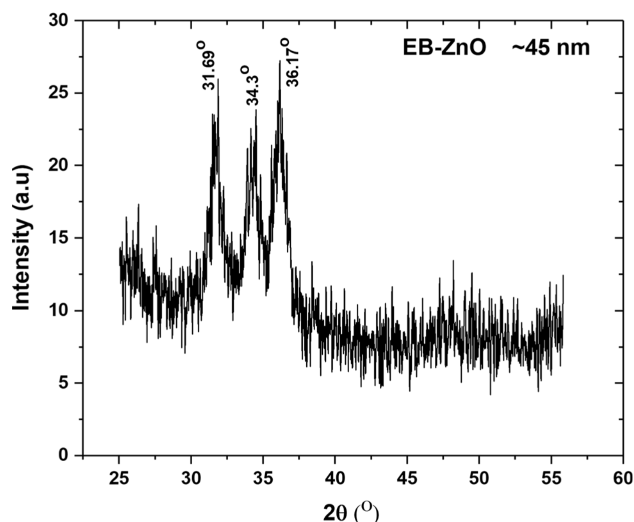

Fig. 2. XRD diffractogram of ZnO thin films deposited on silicon substrate using EB method.

These diffractograms were used to deduce the lattice constants a and c of the ZnO crystal lattice based on the distance between lattice planes (d_{hkl}) using Bragg's law,[7]

$$2d_{hkl}\sin\theta = \lambda, \tag{1}$$

where θ is Bragg's angle, 2θ is the scattering angle, and λ is the x-ray wavelength (1.54 Å for the Cu K_α line). The relation between d_{hkl} and the lattice constants a and c for the hexagonal structure is[7]

$$\frac{1}{d_{hkl}^2} = \frac{4(h^2+hk+k^2)}{3a^2} + \frac{l^2}{c^2}, \tag{2}$$

where h, k, and l are the Miller indices. Based on Eq. 2, a plot of $1/d^2$ against l^2 is shown in Fig. 3, with a linear fit performed to calculate the lattice parameters. The fit yielded average values for the lattice parameters of $a \pm \Delta a = 3.266 \pm 0.007$ Å, $c \pm \Delta c = 5.214 \pm 0.001$ Å for the first sample with thickness of 200 nm and $a \pm \Delta a = 3.266 \pm 0.009$ Å, $c \pm \Delta c = 5.210 \pm 0.017$ Å for the second sample with thickness of 120 nm. These values are slightly larger than those for ZnO powder published in JCPDS card no. 36-1451 (a_0 = 3.2498 Å, c_0 = 5.2066 Å). Lattice constants are usually influenced by the substrate and impurities in the sample. The slightly larger values obtained in this work are mainly due to incorporation of Cl into the ZnO crystal lattice, since the samples contain chlorine, as confirmed by the XRF measurements presented below. Because chlorine has ionic radius of 1.81 Å while oxygen has ionic radius of 1.35 Å,[31] Cl replaces O in the ZnO crystal lattice, which will cause expansion of the lattice parameters. For undoped ZnO nanorods and branched microrods on Si substrate, Lupan et al.[32] found a = 0.3249 nm and c = 0.5206 nm, being smaller than the values reported herein, in support of the aforementioned explanation.

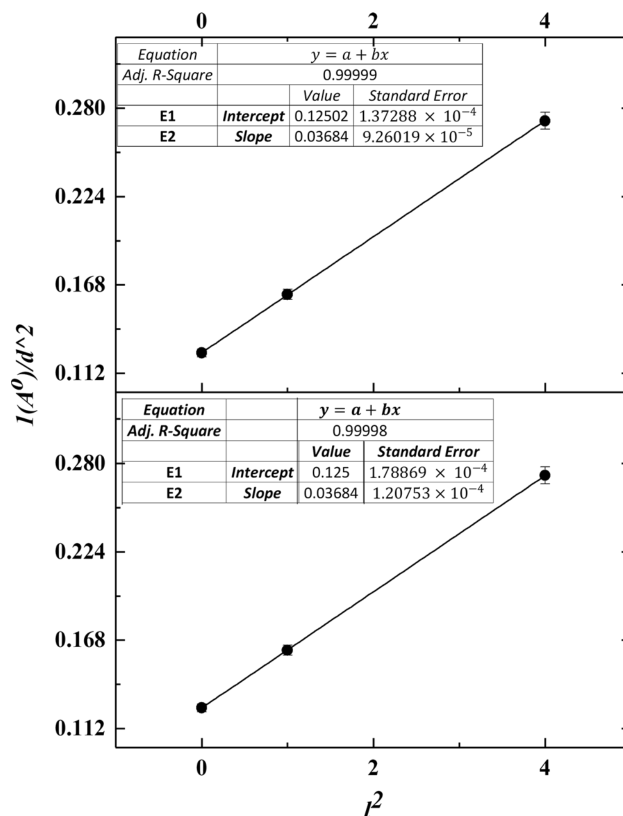

Equation		$y = a + bx$
Adj. R-Square		0.99999
		Value	Standard Error
E1	Intercept	0.12502	1.37288×10^{-4}
E2	Slope	0.03684	9.26019×10^{-5}

Equation		$y = a + bx$
Adj. R-Square		0.99998
		Value	Standard Error
E1	Intercept	0.125	1.78869×10^{-4}
E2	Slope	0.03684	1.20753×10^{-4}

Fig. 3. Plot of $1/d^2$ against l^2 with linear fits for sample 1 (upper) and sample 2 (lower).

The stress in the deposited films was determined using the relation[31,33]

$$\varepsilon(002) = (c - c_0) \times 100\%/c_0, \tag{3}$$

where c is the calculated lattice constant of the hexagonal structure of the ZnO microrods and c_0 is the standard value (from JCPDS card no. 36-1451) of the unstrained lattice constant of ZnO material. This percentage was found to be 0.154% for the first sample (t = 200 nm) and 0.077% for the second sample (t = 120 nm).

Figure 4 shows the morphological features of the as-prepared ZnO samples. The surface of the substrate was covered with ZnO microrods. The microrods in both images are hexagonal and appear perpendicular to the surface of the substrate, a result that is consistent with the XRD diffractograms shown in Fig. 1 with preferential (002) orientation. Figure 4b shows nanowires with length of 200 nm to 400 nm and diameter of 20 nm to 50 nm extending out from the edges of several microrods. It is expected that these nanowires form in the vicinity of Zn^{+2} and O^{-2} due to the large ionicity of the bonds between the zinc and oxygen atoms.[2]

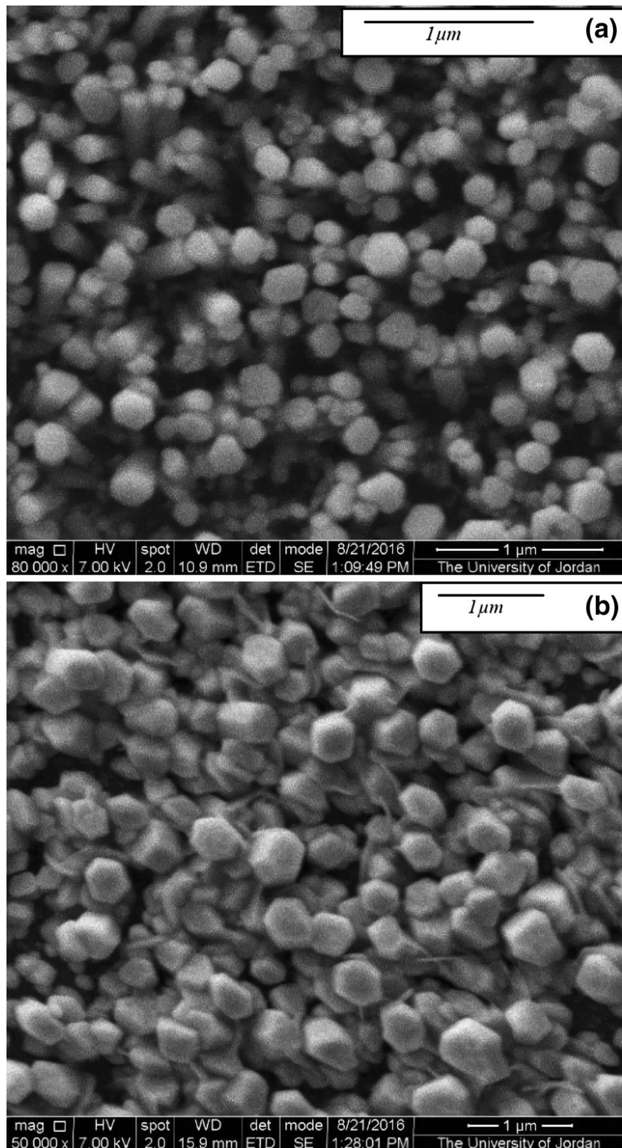

Fig. 4. SEM images of the two as-deposited ZnO films on Si substrate: (a) sample 1 and (b) sample 2.

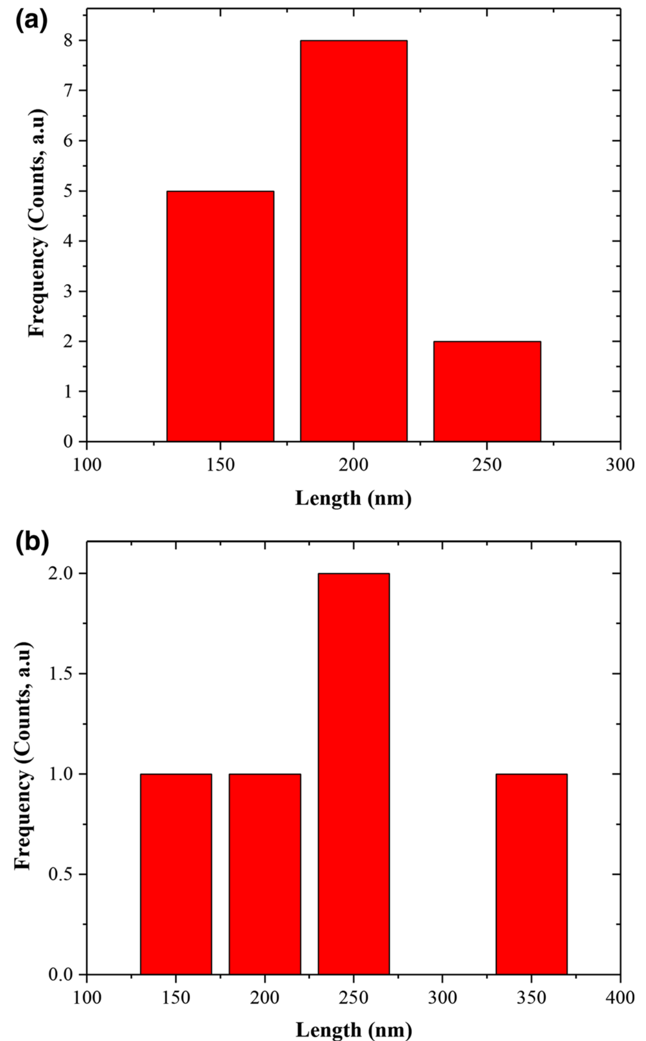

Fig. 5. Histograms of length distribution from SEM images: (a) Fig. 4a and (b) Fig. 4b.

ImageJ software was used to estimate the length and diameter of the rods, yielding an average length of 170 ± 31 nm from Fig. 4a and 210 ± 62 nm from Fig. 4b. The average diameter of the microrods was 170 ± 43 nm and 220 ± 40 nm for Fig. 4a and b, respectively. Figure 5 shows histograms of the length distribution for the two samples, while Fig. 6 displays histograms of the diameter distribution for both samples.

The composition of the samples was explored using x-ray fluorescence (XRF). Table I presents the XRF results for samples 1 and 2. The large SiO_2 percentage in both samples is due to the use of Si substrate, as the native SiO_2 surface layer on the Si substrate is clearly seen in the XRF measurements. The results in this table show that the ZnO content of sample 1 was larger than that of sample 2, which can be related to the difference in film thickness, while the ratio of Cl to ZnO content was as high as 0.90 in sample 1, compared with 0.26 in sample 2. Also, the CaO content of sample 2 was much smaller than that of sample 1, while sample 1 contained K_2O and sample 2 contained Fe_2O_3. The presence of Cl is due to use of $ZnCl_2$ starting material, while the other foreign contents of the films are due to impurities in the $ZnCl_2$, which had purity of 99%. These differences in the composition of the films prepared from the same solution are partially due to the difference in film thickness, but mainly due to the dynamic nature of the spray pyrolysis method; That is, films prepared under the same conditions from the same solution will not necessarily have exactly the same composition. The composition of the films drastically affects their properties.

Figure 7 shows the EDS spectra of the films, where both parts of the figure show the presence of Zn, O, and Si. The EDS results indicate O:Si:Zn concentration ratios of 46.46:41.83:11.72 (at.%) for

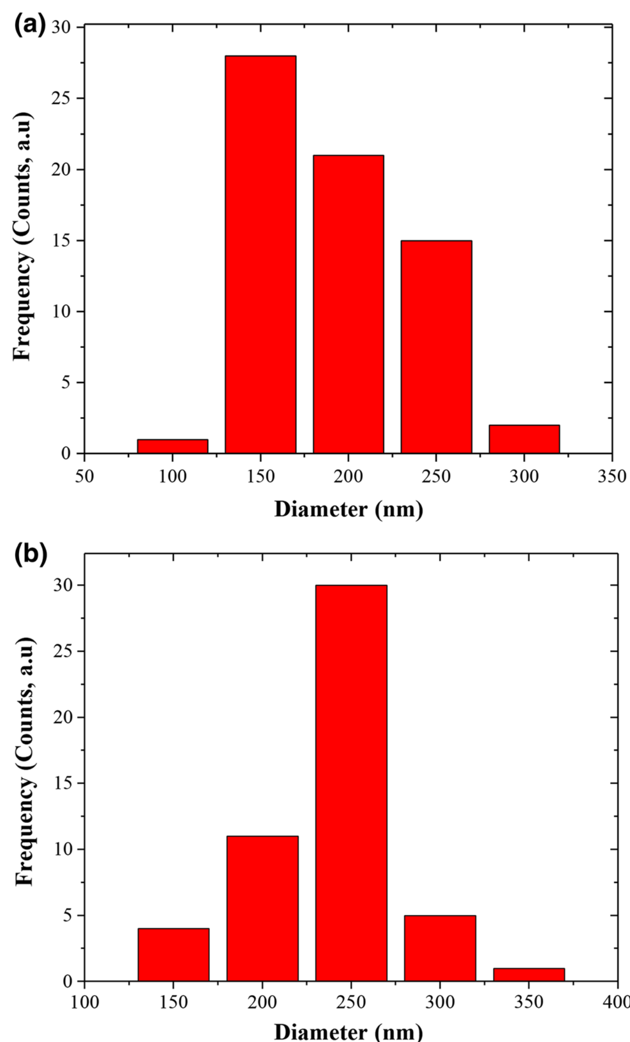

Fig. 6. Histograms of diameter distribution from SEM images: (a) Fig. 4a and (b) Fig. 4b.

Table I. XRF results for samples 1 and 2

Sample 1		Sample 2	
Analyte	**Result (%)**	**Analyte**	**Result (%)**
SiO_2	99.6290	SiO_2	99.8531
ZnO	0.1769	ZnO	0.1091
Cl	0.1595	Cl	0.0283
K_2O	0.0201	CaO	0.0066
CaO	0.0145	Fe_2O_3	0.0029

sample 1 and 39.85:53.43:6.72 (at.%) for sample 2. As seen in Table I, SiO_2 has the largest content due to the Si substrate, so the high oxygen content in the EDS results is partitioned between all oxides in Table I, with the largest part corresponding to SiO_2. This clearly indicates that Si is only partially bonded to oxygen. Hence, what is found in the samples is SiO_x, with $x < 2$. This observation leads to the conclusion that the samples are oxygen deficient.

The chemical bonding, compositional quality, and functionalities of the ZnO thin films were studied using FTIR spectroscopy. The FTIR spectra of the deposited samples are shown in Fig. 8, comparing those deposited by SP with the control sample deposited by EB. The ZnO identity of the thin EB film was first confirmed by XRD measurements, as mentioned above. The figure shows a clear correspondence between the FTIR spectra for the samples deposited using the two techniques, viz. SP and EB, further confirming that the SP films were mainly composed of ZnO. The stretching vibration of Zn–O bond was reflected by the presence of peaks at 420 cm^{-1}, 454 cm^{-1}, 485 cm^{-1}, and 546 cm^{-1}, while the substrate's Si–O stretching vibration is observed at around 1072 cm^{-1}. These values can be compared with the positions of corresponding vibrations found by Foo et al.[34] for nanostructured ZnO thin films produced on silver electrodes grown on SiO_2/Si substrates by the sol–gel method. Foo et al. found the stretching vibration of Zn–O bond at $\sim$ 458 cm^{-1} and the stretching frequency of Si–O bond at $\sim$ 1092 cm^{-1}. Similar band positions have also been reported by many other researchers.[35–42] The vibrational peaks between 1400 cm^{-1} and 1700 cm^{-1} are usually attributed to carboxyl groups coordinated to metal ions, such as Zn in this case; specifically, the peak at around 1621 cm^{-1} is usually assigned to Zn carboxylate.[39,42–44] The small variations in peak positions are attributed to changes in the chemical environment of the different bonds due to the different precursors and different deposition techniques used to prepare the ZnO thin films. The small differences can also be traced to impurities that may exist in the different precursors. These shifts can easily be seen in Fig. 8, where the SP samples are compared with those deposited by EB evaporation.

Figure 9 shows the percent reflectance spectra of the two ZnO films as a function of photon wavelength λ. The percent reflectance ($R\%$) of the ZnO thin films decreased as the wavelength of the incident radiation was increased, with the maximum reflectance observed in the ultraviolet (UV) region, reaching 42.75% for sample 1 and 18.92% for sample 2. $R\%$ decreased with λ until becoming approximately constant at about 22.50% and 11.34% for sample 1 and 2 respectively. Two maxima are observed in the reflectance spectra of both samples at $\lambda = 277.3$ (4.47 eV) and 367.3 nm (3.37 eV). These peaks are expected to represent the absorption edges of SiO_x where $x \approx 1.5$.[38]

Figure 10 shows the room-temperature photoluminescence spectra of the microrod ZnO films, showing four evident emission bands. One band lies in the UV region in the range of 340 nm to 384 nm, being related to near-band emission (NBE) resulting from recombination of free excitons,[36] while the three bands in the visible region are due to various

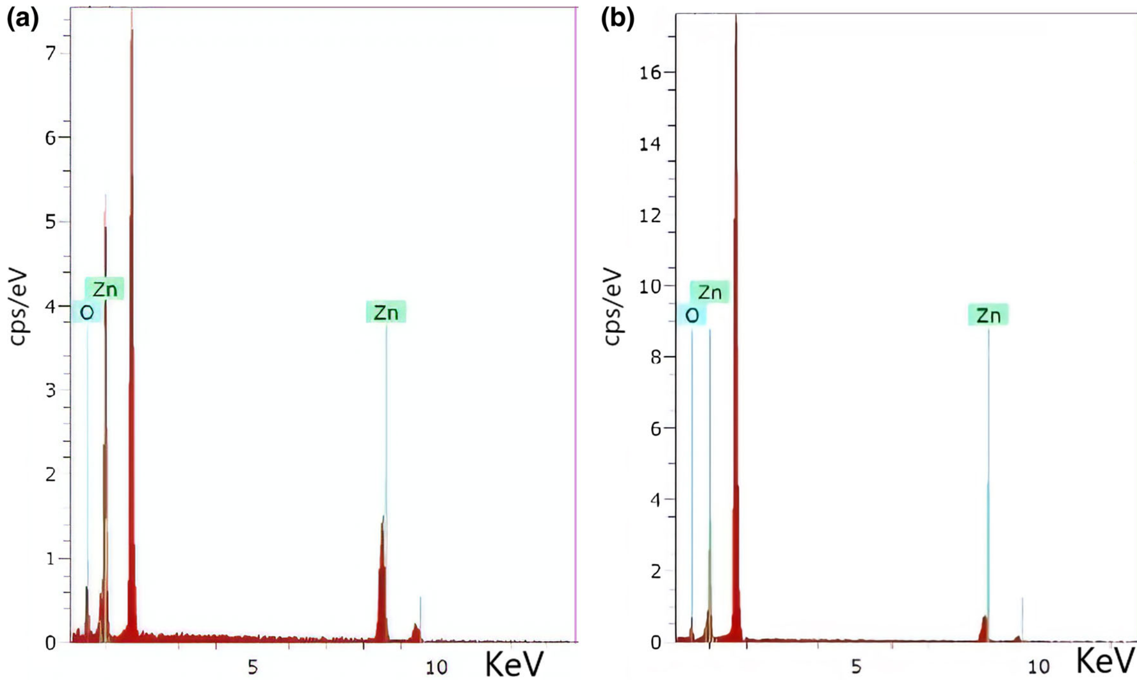

Fig. 7. EDS spectra of ZnO films on Si substrate: (a) sample 1 and (b) sample 2.

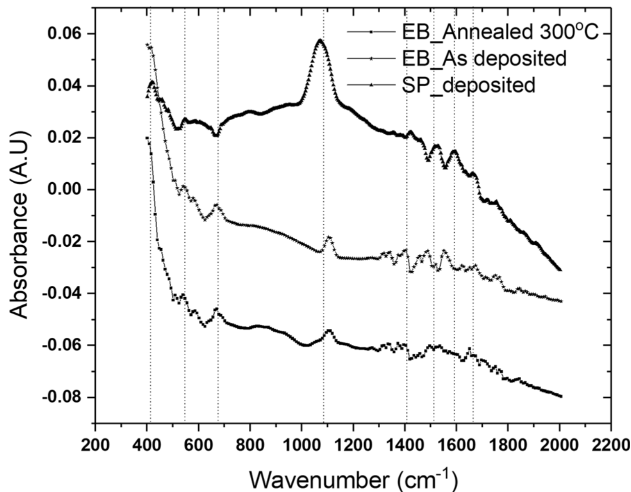

Fig. 8. FTIR absorption spectra of ZnO thin films deposited by SP and EB on silicon substrate.

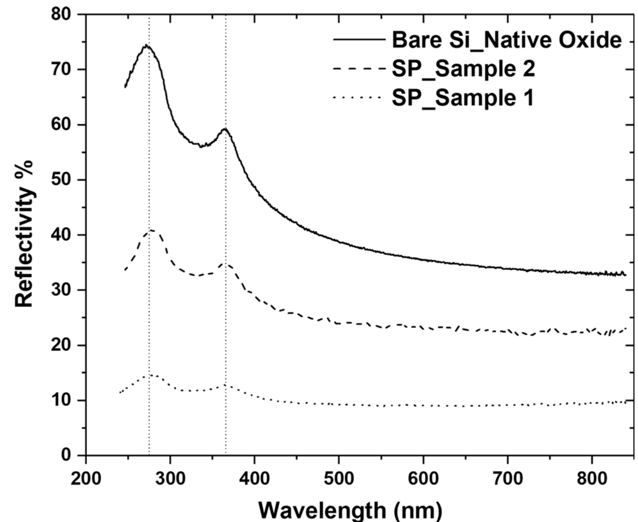

Fig. 9. Percent reflectance spectra of ZnO thin films compared with bare Si substrate.

types of defects and impurities.[37] The visible emissions are in the violet region in the range of 384 nm to 420 nm, blue region from 450 nm to 510 nm, and green region from 510 nm to 565 nm. The UV band of sample 1 consists of four peaks at 344.0 nm, 362.0 nm, 373.9 nm, and 378.0 nm, while for sample 2 it consists of five peaks at 346.0 nm, 356.0 nm, 363.0 nm, 378.0 nm, and 384.0 nm. The violet band of sample 1 consists of five peaks at 389.1 nm, 392.0 nm, 396.0 nm, 400.0 nm, and 408.9 nm, while for sample 2 it consists of three peaks at 393.1 nm, 396.0 nm, and 408.0 nm. The blue band of sample 1 consists of two peaks at 475.0 nm and 485.0, nm, while that of sample 2 consists of three peaks at 471.1 nm, 475.0 nm, and 483.9 nm. The green band for both samples consists of eight peaks each. For sample 1 these peaks are at 496.0 nm, 508.0 nm, 521.9 nm, 534.0 nm, 538.0 nm, 547.0 nm, 550.0 nm, and 558.0 nm, while for sample 2 these peaks are at 495.1 nm, 506.0 nm, 521.9 nm, 531.0 nm, 538.0 nm, 545.0 nm, 551.9 nm, and 565.0 nm. Note that some peaks have exactly the same positions for the two samples. Other peaks of sample 1 (blue and green)

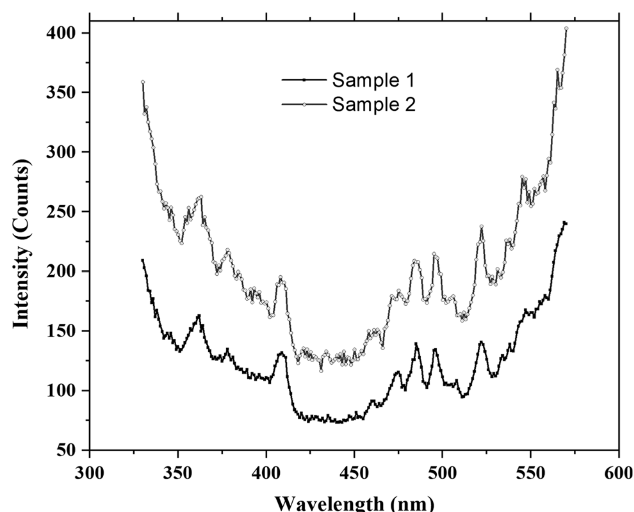

Fig. 10. Room-temperature photoluminescence spectra of ZnO films on Si substrate.

are shifted towards longer wavelength relative to corresponding peaks of sample 2. The opposite is true for the ultraviolet peaks, but the shift is slightly more apparent for the violet band. Some peaks appeared in the spectrum of sample 2 but not in that of sample 1, and vice versa. These differences are expected to be due to the differences in thickness, microrod size, and impurity types and concentration.

Room-temperature photoluminescence (PL) spectra are usually considered to represent a quality indicator for a material under investigation, because of the valuable information they can provide in connection to optically active defects and/or relaxation pathways. Hence, the characteristic PL signal might represent defect emissions or may be considered a direct consequence of band-edge luminescence. The PL spectra of the as-prepared ZnO films suggest that the UV luminescence is associated with near-band-edge transitions. The presence of different nanosize particles within the films is evident from the several peaks in the UV region. Moreover, the visible part of the emission spectrum can be attributed to various defects in the zinc oxide crystal structure, including ionic vacancies and interstitials as well as other extrinsic impurities. Also, the blue emission is usually related to zinc interstitials and/or vacancies. Finally, the green emission, which is commonly connected to singly ionized oxygen vacancies, is easily influenced by surface modification.

CONCLUSIONS

Microrod-structured hexagonal (wurtzite-type) ZnO films were prepared on silicon substrate using SP and EB methods. XRD analysis revealed preferential (002) orientation for the SP-deposited films, indicating crystal growth perpendicular to the substrate. SEM images confirmed the XRD results, showing hexagonal microrods perpendicular to the substrate. XRF analysis showed that the SP films were basically ZnO thin films with traces of other compounds coming from impurities in the precursor in addition to SiO_2 from the silicon substrate. EDS analysis confirmed presence of Zn and O in addition to Si. The high concentration of oxygen is due to presence of other oxides such as SiO_2. FTIR absorption spectra exhibited peaks corresponding to ZnO stretching and that of Si–O. The percent reflectance of the samples showed a decreasing trend with wavelength with two maxima related to the absorption edges of SiO_x with $x < 2$. The PL spectra showed four bands, one in the UV and three in the visible part of the spectrum, corresponding to blue, violet, and green. The band in the UV is related to near-band-edge emissions, whereas those in the visible range are related to impurities and defects.

REFERENCES

1. H.A. Ali, A.A. Iliadis, R.F. Mulligan, A.V.W. Cresce, P. Kofinas, and U. Lee, *Solid State Electron.* 46, 1639 (2002).
2. A. Kamalianfar, S.A. Halim, M.G. Naseri, M. Navasery, F.U. Din, J.A.M. Zahedi, K.P. Lim, E.B. Saion, C.K. Chen, and A.L. Monfared, *Int. J. Electrochem. Sci.* 8, 7724 (2013).
3. Y. Zou, Z. Qi, W. Jiang, J. Duan, and Z. Ma, *Mater. Lett.* 199, 57 (2017).
4. P.M. Verghese and D.R. Clarke, *J. Appl. Phys.* 87, 4430 (2000).
5. R.K. Thareja and A. Mitra, *Appl. Phys. B Lasers Opt.* 71, 181 (2000).
6. S. Ueno and S. Fujihara, *Int. J. Photoenergy* (2012). https://doi.org/10.1155/2012/268173.
7. C. Shi, K. Xiang, Y. Zho, X. Chen, W. Zhou, and H. Chen, *Electrochem. Acta* 246, 1088 (2017).
8. G.A. Velázquez-Nevárez, J.R. Vargas-García, J. Aguilar-Hernández, O.E. Vega-Becerra, F. Chen, Q. Shen, and L. Zhang, *Mater. Res.* 19, 113 (2016).
9. N. Ekthammathat, A. Phuruangrat, S. Thongtem, and T. Thongtem, *Dig. J. Nanomater. Biostruct.* 10, 149 (2015).
10. Y. Chen, H.-J. Ko, S.-K. Hong, Y. Segawa, and T. Yao, *Appl. Phys. Lett.* 80, 1358 (2002).
11. D.S. Kang, S.K. Han, S.M. Yang, J.G. Kim, W.J. Hwang, and S.K. Hong, *J. Korean Phys. Soc.* 53, 292 (2008).
12. S. Nicolay, M. Benkhaira, L. Ding, J. Escarre, G. Bugnon, F. Meillaud, and C. Ballif, *Sol. Energy Mater. Sol. Cells* 105, 46 (2012).
13. S. Faÿ, J. Steinhauser, S. Nicolay, and C. Ballif, *Thin Solid Films* 518, 2961 (2009).
14. A. Hongsingthong, I.A. Yunaz, S. Miyajima, and M. Konagai, in *Proceedings of the 35th IEEE Photovoltaic Specialists Conference* (2010), p. 1508.
15. O. Kluth, G. Schöpe, J. Hüpkes, C. Agashe, J. Müller, and B. Rech, *Thin Solid Films* 442, 80 (2003).
16. S.J. Ikhmayies, N.M. Abu El-Haija, and R.N. Ahmad-Bitar, *Phys. Scr.* 81, 015703 (2010).
17. F. Kadi Allah, S.Y. Abe, C.M. Nunez, A. Khelil, L. Cattin, M. Morsli, J.C. Bernede, A. Bougrine, M.A. del Valle, and F.R. Diaz, *Appl. Surf. Sci.* 253, 9241 (2007).
18. I. Soumahoro, G. Schmerber, A. Douayar, S. Colis, M. Abd-Lefdil, N. Hassanain, A. Berrada, D. Muller, A. Slaoui, H. Rinnert, and A. Dinia, *J. Appl. Phys.* 109, 033708 (2011).
19. K. Vijayalakshmi, K. Karthick, and D. Gopalakrishna, *Ceram. Int.* 39, 4749 (2013).
20. S.J. Ikhmayies and M.B. Zbib, *J. Electron. Mater.* 46, 3982 (2017).
21. P.V. Raghavendra, J.S. Bhat, and N.G. Deshpande, *Mater. Sci. Semicond. Process.* 68, 262 (2017).

22. H.K. Juwhari, S.J. Ikhmayies, and B. Lahlouh, *Int. J. Hydrog. Energy* 42, 17741 (2017).
23. P. Petkova, L. Nedelchev, D. Nazarova, K. Boubaker, and R. Bachvarova, *Optik* 139, 217 (2017).
24. C.A. Schneider, W.S. Rasband, and K.W. Eliceiri, *Nat. Methods* 9, 671 (2012).
25. J. Schindelin, C.T. Rueden, M.C. Hiner, and K.W. Eliceiri, *Mol. Reprod. Dev.* 82, 518 (2015).
26. K. Zheng, Q. Guo, and E.G. Wang, *Surf. Sci.* 602, 2600 (2008).
27. J.M. Jensen, A.B. Oelkers, R. Toivola, and D.C. Johnson, *Chem. Mater.* 14, 2276 (2002).
28. C.S. Ku, H.Y. Lee, J.M. Huang, and C.M. Lin, *Mater. Chem. Phys.* 120, 236 (2010).
29. D.C. Agarwal, R.S. Chauhan, A. Kumar, D. Kabiraj, F. Singh, S.A. Khan, D.K. Avasthi, J.C. Pivin, M. Kumar, J. Ghatak, and P.V. Satyam, *J. Appl. Phys.* 99, 123105 (2006).
30. P. Mitra and S. Mondal, *Prog. Theor. Exp. Phys.* 1, 17 (2013).
31. R.D. Shannon, *Acta Cryst. A* 32, 751 (1976).
32. O. Lupan, L. Chow, G. Chai, B. Roldan, A. Naitabdi, A. Schulte, and H. Heinrich, *Mater. Sci. Eng. B* 145, 57 (2007).
33. J.J. Hassan, M.A. Mahdi, A. Ramizy, H.A. Hassan, and Z. Hassan, *Superlattices Microstruct.* 53, 31 (2013).
34. K.L. Foo, M. Kashif, U. Hashim, and M.E. Ali, *Curr. Nanosci.* 9, 000 (2013).
35. A. Barranco, F. Yubero, J.P. Espinós, P. Groening, and A.R. González-Elipe, *J. Appl. Phys.* 97, 113714 (2005).
36. X. Wang, Q. Li, Z. Zhang, Z. Liu, and J. Zhang, *Appl. Phys. Lett.* 84, 4941 (2004).
37. Y.C. Kong, D.P. Yu, B. Zhang, W. Fang, and S.Q. Feng, *Appl. Phys. Lett.* 78, 407 (2001).
38. A.R. Nimbalkar and M.G. Patil, *Phys. B* 527, 7 (2017).
39. A. Djelloul, M.-S. Aida, and J. Bougdira, *J. Lumin.* 130, 2113 (2010).
40. T. Ivanova, A. Harizanova, T. Koutzarova, and B. Vertruyen, *Mater. Lett.* 64, 1147 (2010).
41. X.Q. Wei, Z. Zhang, Y.X. Yu, and B.Y. Ma, *Opt. Laser Technol.* 41, 530 (2009).
42. P.C. Yao, S.T. Hang, Y.S. Lin, W.T. Yen, and Y.C. Lin, *Appl. Surf. Sci.* 257, 1441 (2010).
43. V. Zeleňák, Z. Vargová, and K. Györyová, *Spectrochem. Acta A* 66, 262 (2007).
44. V. Otero, D. Sanches, C. Montagner, M. Vilarigues, L. Carlyle, J.A. Lopes, and M.J. Melo, *J. Raman Spectrosc.* (2014). https://doi.org/10.1002/jrs.4520.